Electronic supplement

Burkhardt et al. (2014): Evidence for Mo isotope fractionation in the solar nebula and during planetary differentiation

S1: Nucleosynthetic Mo isotope anomalies in CK (Karoonda), CM (Murchison) and CO (Kainsaz) chondrites

For samples that were not analyzed for nucleosynthetic Mo isotope anomalies in our previous study (Burkhardt et al., 2011), we obtained Mo isotope data on unspiked aliquots of the sample powders. Similar sample weights, digestion procedures and ion chromatographic methods were used for both the unspiked and spiked samples. Note that all lab ware was kept strictly separate for the unspiked and spiked samples. The Mo isotope measurements on the unspiked samples in the present study were performed using the Thermo *NeptunePlus* MC-ICP-MS at the University of Münster, equipped with standard H cones and a different Cetac AridusII desolvator than that used for double-spike work. We have not noticed any memory effect when switching between unspiked and spiked setups. Furthermore, any such unnoticeably small effect would have been corrected for by the on-peak-zero baseline measurements. Instrumental and natural mass-dependent isotope fractionation was corrected by internal normalization to $^{98}Mo/^{96}Mo=1.453171$ to facilitate comparison to our earlier internally normalized Mo isotope data. The Mo isotope data were also normalized to $^{97}Mo/^{95}Mo=0.602083$, which is necessary when using these data to correct the $\delta^{98/95}Mo$ values obtained from the spiked samples for nucleosynthetic isotope anomalies. The Mo isotope data for the unspiked samples are reported in the ε-notation relative to the Mo isotope composition of the two bracketing Mo standard measurements (Table S1).

Table S1: Nucleosynthetic Mo isotope anomalies for CM, CO and CK chondrites.

Sample		N	$\varepsilon^{92}Mo$	$\varepsilon^{94}Mo$	$\varepsilon^{95}Mo$	$\varepsilon^{96}Mo$	$\varepsilon^{97}Mo$	$\varepsilon^{98}Mo$	$\varepsilon^{100}Mo$
			internal normalization to $^{98}Mo/^{96}Mo=1.453171$						
Murchison	CM2	3	5.10 ± 0.22	2.33 ± 0.90	1.42 ± 0.22	0	1.65 ± 0.25	0	2.07 ± 0.28
Kainsaz	CO3	3	2.41 ± 0.15	1.66 ± 0.34	1.39 ± 0.34	0	0.71 ± 0.28	0	0.97 ± 0.11
Karoonda	CK4	3	2.16 ± 0.85	1.55 ± 0.36	1.07 ± 0.90	0	1.15 ± 0.80	0	0.64 ± 0.66
			internal normalization to $^{97}Mo/^{95}Mo=0.602083$						
Murchison	CM2	3	4.04 ± 0.58	1.03 ± 0.95	0	-1.53 ± 0.22	0	-1.76 ± 0.31	0.09 ± 0.19
Kainsaz	CO3	3	-0.02 ± 1.06	-0.07 ± 0.69	0	-1.05 ± 0.14	0	-0.38 ± 0.53	1.25 ± 0.97
Karoonda	CK4	3	1.20 ± 2.62	0.51 ± 1.42	0	-1.11 ± 0.19	0	-1.18 ± 1.60	-0.61 ± 3.78

N= number of analysis of sample solution. Instrumental and natural mass-dependent fractionation was corrected by internal normalization to $^{98}Mo/^{96}Mo=1.453171$ or $^{97}Mo/^{95}Mo=0.602083$, using the exponential law. $\varepsilon^{i}Mo= [(^{i}Mo/^{9x}Mo)_{sample}/(^{i}Mo/^{9x}Mo)_{standard} -1]\times10^4$ with x = 6 or 5. Uncertainties were calculated using $\sigma t_{0.95,n-1}/\sqrt{n}$.

All analyzed chondrites show nucleosynthetic Mo isotope anomalies relative to the terrestrial standard (Figure S1). The anomaly patterns are consistent with variable deficits in *s*-process Mo and confirm our previous conclusion that all chondrite groups are depleted in *s*-process Mo relative to the Earth (Burkhardt et al., 2011). The Mo isotope anomalies of the analyzed Murchison sample are slightly smaller than those obtained for another Murchison sample in our previous study (ε^{92}Mo=5.10±0.22 here *vs*. 6.44±0.39 in Burkhardt et al. 2011). This most likely reflects small Mo isotope heterogeneities at the sampling scale. For Kainsaz the Mo isotope anomalies are slightly larger than those reported by Burkhardt et al. (2011) for another CO3 chondrite (NWA 2090), and this might be due to terrestrial weathering of the latter. For Karoonda we provide the first Mo isotope data, indicating that the Mo isotope anomalies for CK chondrites are comparable to those of the CO, CR and CB chondrites.
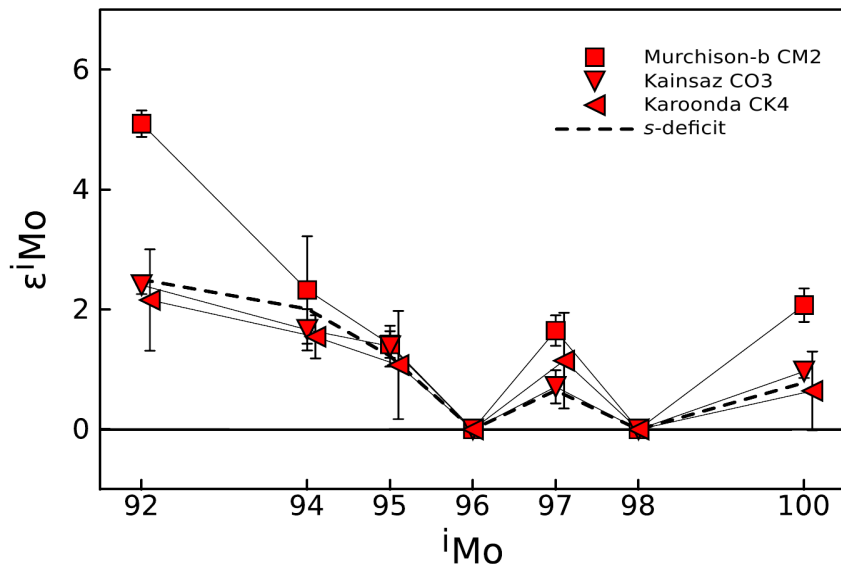
Figure S1: ^{i}Mo vs. ε^iMo plot for CM, CO, and CK chondrites. Data are internally normalized to ^{98}Mo/^{96}Mo. Dashed *s*-process deficit pattern was calculated using the stellar model of *s*-process nucleosynthesis (Arlandini et al., 1999) and was scaled to fit the Kainsaz data.

S2: Correcting measured δ$^{98/95}$Mo for nucleosynthetic Mo isotope anomalies

The Mo stable isotope data are given as δ$^{98/95}$Mo values calculated relative to the NIST SRM 3134 Mo standard, where δ$^{98/95}$Mo$_{measured}$ represents the measured isotope fractionation as obtained from the double spike inversion, while δ$^{98/95}$Mo$_{corrected}$ is the purely mass-dependent isotope fractionation obtained after correction for mass-independent (*i.e.*, nucleosynthetic) isotope anomalies. The double spike inversion of a sample run iteratively calculates a fractionation factor α relative to the SRM 3134 standard by assuming that the difference in the isotopic composition of the sample and the standard is entirely mass-dependent. However, for samples having mass-independent isotope anomalies relative to the standard, such as iron meteorites and chondrites (Burkhardt et al., 2011; Dauphas et al., 2002) this routine will lead to false

α values and thus to incorrect $\delta^{98/95}$Mo. The $\delta^{98/95}$Mo$_{measured}$ values, therefore, must be corrected for nucleosynthetic isotope effects to obtain the purely mass-dependent Mo isotope fractionation. To correct for the effects of nucleosynthetic Mo isotope anomalies on measured $\delta^{98/95}$Mo values the isotopic composition of the unspiked samples must be known. For the samples Karoonda, Murchison-b and Kainsaz this information was obtained by analyzing unspiked aliquots (Table S1). For most of the other samples analyzed here, this information is available from our previous Mo isotope study (Burkhardt et al., 2011).

The effects of nucleosynthetic isotope anomalies can be corrected using two different approaches. The first uses the unspiked Mo isotope compositions of the samples instead of that of the SRM 3134 standard in the double spike inversion to obtain "absolute" isotope abundances of the samples (Niederer et al., 1985). Normalizing these abundances to the SRM 3134 standard and subtracting the mass-independent effects then gives the pure mass-dependent fractionation (relative to the SRM 3134 standard). In the second approach the measured $\delta^{98/95}$Mo values obtained from the double spike inversion using the SRM 3134 standard composition are subsequently corrected for mass-independent effects by an equation that relates the true fractionation, measured fractionation and the independently measured nucleosynthetic isotope anomalies. Such equations can be obtained by modeling the effects of nucleosynthetic (*s*-process) anomalies on the measured mass-fractionation. We employed both correction methods and they yield identical results, as exemplified for the IVB irons in the following sections before we provide a more general discussion about separating mass-dependent and mass-independent effects in the Mo system.

S2.1 Correcting measured $\delta^{98/95}$Mo by modeling the effects of nucleosynthetic anomalies.

The nucleosynthetic Mo isotope anomalies in bulk meteorites are caused by a heterogeneous distribution of *s*-process Mo (Burkhardt et al., 2011; Dauphas et al., 2002). We therefore modeled the changes in $\delta^{98/95}$Mo$_{measured}$ as a function of the size of the nucleosynthetic anomalies by subtracting various amounts of *s*-process Mo (Arlandini et al., 1999) from the Mo isotope abundances of the SRM 3134 standard. For internal normalization to ^{97}Mo/^{95}Mo=0.602083, this subtraction results in the anomaly patterns shown in Fig. S2a. The magnitude of the generated anomalies increase linearly with the size of the *s*-process deficit; *e.g.*, a deficit of 0.005% *s*-process Mo corresponds to an ϵ^{96}Mo$_{(7/5)nucleosynthetic}$ of -0.86, while a deficit of 0.05% *s*-process Mo results in an ϵ^{96}Mo$_{(7/5)nucleosynthetic}$ of -8.6 (Table S2). The modeled anomalies are then translated into isotope abundances which are used in the double spike inversion as if these calculated abundances (*i.e.,* SRM abundance with subtraction of modeled amount of *s*-process isotopes) were a sample. The inversion results in a $\delta^{98/95}$Mo$_{measured}$ that is fractionated relative to the SRM standard (Fig. S2b). A *s*-deficit of 0.01% thus induces an apparent Mo isotope fractionation of $\delta^{98/95}$Mo$_{measured}$ =

-0.12‰. The magnitude of the apparent fractionation is linearly correlated with the size of the *s*-process anomaly. From this numerical experiment we therefore obtain the parameterized relationship:

$$\delta^{98/95}Mo_{corrected} = \delta^{98/95}Mo_{measured} - \varepsilon^{96}Mo_{(7/5)nucleosynthetic} \times 0.066$$

where $\varepsilon^{96}Mo_{(7/5)nucleosynthetic}$ is the nucleosynthetic anomaly for $\varepsilon^{96}Mo$ normalized to $^{97}Mo/^{95}Mo$. Similar relations can also be obtained for other anomalies (*e.g.*, $\varepsilon^{95}Mo$ $\varepsilon^{98}Mo$, $\varepsilon^{100}Mo$), but we use the $\varepsilon^{96}Mo$ for the $^{97}Mo/^{95}Mo$ normalization, because *s*-deficits result in readily resolvable anomalies on $\varepsilon^{96}Mo$, which is furthermore the most precisely measured isotope anomaly in this normalization scheme.
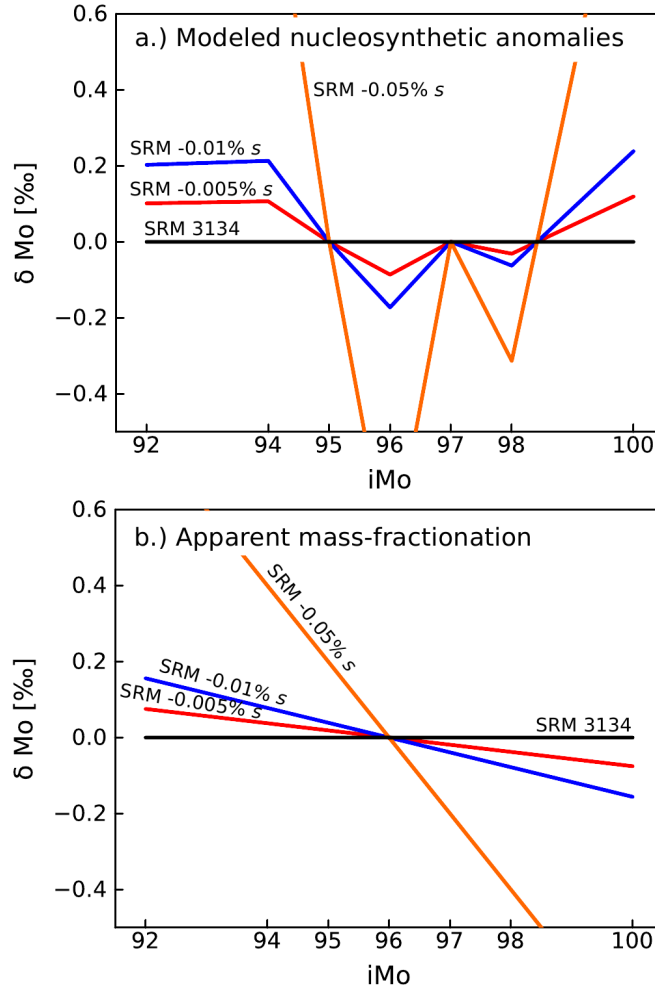
Fig. S2. Modeled effect of nucleosynthetic anomalies (*s*-process variations) on the mass-fractionation obtained by double-spike deconvolution relative to the SRM 3134 Mo standard. a.) Subtracting *s*-process Mo (Arlandini et al., 1999) from the terrestrial Mo isotope composition (given by the SRM 3134 Mo standard) and internal normalization to $^{97}Mo/^{95}Mo= 0.602083$ results in characteristic anomaly patterns scaling linearly with the size of *s*-process deficit. b.) Apparent mass fractionation obtained from the double-spike deconvolution of modeled mass-independent effects relative to the SRM standard. The larger the *s*-process deficit, the larger the apparent mass-fractionation. The relation is parameterized by: $\delta^{98/95}Mo_{corrected} = \delta^{98/95}Mo_{measured} - \varepsilon^{96}Mo_{(7/5)nucleosynthetic} \times 0.066$.

Table S2: Modeled *s*-process anomalies and their induced apparent Mo isotope fractionation

	SRM 3134 Mo	-0.005% s	-0.01% s	-0.05% s
	modeled nucleosynthetic anomalies			
$\varepsilon^{92}Mo$	0.00	1.01	2.03	10.14
$\varepsilon^{94}Mo$	0.00	1.07	2.13	10.67
$\varepsilon^{95}Mo$	0.00	0.00	0.00	0.00
$\varepsilon^{96}Mo$	0.00	-0.86	-1.72	-8.63
$\varepsilon^{97}Mo$	0.00	0.00	0.00	0.00
$\varepsilon^{98}Mo$	0.00	-0.31	-0.63	-3.13
$\varepsilon^{100}Mo$	0.00	1.19	2.38	11.93
	modeled isotope abundances			
^{92}Mo	14.7339	14.7352	14.7365	14.7468
^{94}Mo	9.2129	9.2137	9.2146	9.2214
^{95}Mo	15.8922	15.8920	15.8918	15.8900
^{96}Mo	16.6717	16.6700	16.6683	16.6549
^{97}Mo	9.5685	9.5683	9.5682	9.5671
^{98}Mo	24.2256	24.2245	24.2234	24.2145
^{100}Mo	9.6952	9.6962	9.6972	9.7054
	Isotope abundances obtained for spiked SRM run with modeled isotope abundances in deconvolution			
^{92}Mo	14.7339	14.7341	14.7341	14.7346
^{94}Mo	9.2129	9.2134	9.2138	9.2176
^{95}Mo	15.8922	15.8917	15.8912	15.8867
^{96}Mo	16.6717	16.6700	16.6683	16.6549
^{97}Mo	9.5685	9.5685	9.5686	9.5690
^{98}Mo	24.2256	24.2254	24.2253	24.2242
^{100}Mo	9.6952	9.6969	9.6987	9.7130
	apparent fractionation induced by nucleosynthetic anomalies			
$\delta^{98/95}Mo$	0.00	-0.06	-0.12	-0.60

The IVB iron meteorites show the largest nucleosynthetic anomalies of all iron meteorite classes ($\varepsilon^{96}Mo_{(7/5)nucleosynthetic}$= -0.74±0.03) corresponding to a *s*-process deficit of ~0.0038 % (Burkhardt et al., 2011). The above derived equation implies that the $\delta^{98/95}Mo_{measured}$ for IVB irons thus needs to be corrected by ~0.05‰. For instance, from the double spike inversion relative to the SRM abundances we obtain for the IVB iron meteorite Cape of Good Hope a $\delta^{98/95}Mo_{measured}$ of -0.25±0.06, slightly lighter than what is found for the other magmatic iron meteorites with smaller nucleosynthetic anomalies. A 0.05‰ correction for its nucleosynthetic contribution results in a $\delta^{98/95}Mo_{corrected}$ of -0.20±0.07, which is well within the range of the other magmatic irons, highlighting that the correction is reasonable.

S2.2 Decomposing mass-dependent and mass-independent effects using 'absolute' Mo isotope compositions

The above correction procedure is based on our 'a priori' knowledge of *s*-process deficits in Mo isotopes and their linear effect on apparent mass-dependent fractionation. As an alternative to that correction procedure, we have also used the unspiked Mo isotope data obtained here and by Burkhardt et al. (2011). These data were all internally normalized to $^{97}Mo/^{95}Mo$ = 0.602083 (Lu and Masuda 1994), the same ratio that was also used to calculate the relative Mo isotope abundances of the SRM 3134 standard. Note that ^{97}Mo and ^{95}Mo have very similar *s*-process contributions (58 and 55%), and therefore variations in *s*-process Mo do not significantly affect the $^{97}Mo/^{95}Mo$ ratio. The unspiked Mo isotope abundances thus obtained for each sample were then used in the double spike inversion instead of the

abundances of the SRM 3134 standard. The thereby obtained 'absolute' Mo isotope compositions of the samples include mass-dependent and mass-independent effects. (We put 'absolute' in quotation marks because in our understanding double spiking is a relative method, as the double-spike itself is calibrated relative to some reference composition; see for example Rudge et al., 2009). Subtracting the mass-independent part known from the unspiked run then allows to calculate the pure mass-dependent part of a given sample. Figure S3 and Table S3 illustrates the results obtained from this inversion procedure for the IVB iron meteorite Cape of Good Hope. The nucleosynthetic anomalies for internal normalization to $^{97}Mo/^{95}Mo$ are given in the table and are shown by the red line in Fig. S3a. Calculating isotope abundances from these anomalies and comparing them to the SRM abundances reveal a mass-independent part of $\delta^{98/95}Mo = -0.023‰$. The blue line in Figure S3a shows the $\delta^i Mo$ values relative to the SRM 3134 standard as obtained from inverting the spiked run using the internally normalized IVB abundances as reference. These $\delta^i Mo$ values include both mass-dependent and mass-independent Mo isotope variations and give a $\delta^{98/95}Mo$ of $-0.22‰$. The true mass-dependent fractionation is then obtained as the difference between the blue and the red curve, represented as the black line in Figure S3b ($\delta^{98/95}Mo_{true} = -0.22 - (-0.023) = -0.20‰$). As shown above, the inversion of the spiked sample run with the SRM abundances as reference yields a $\delta^{98/95}Mo_{measured}$ of $-0.25‰$ (green line in Fig S3b). For Cape of Good Hope the difference between these two results corresponds to $\sim 0.05‰$ $\delta^{98/95}Mo$, indicating that for this sample the measured $\delta^{98/95}Mo$ of $-0.25‰$ needs to be corrected upwards to $\delta^{98/95}Mo_{corrected} = -0.20‰$. Decomposing mass-dependent and mass-independent effects using 'absolute' Mo isotope compositions thus gives the same results as obtained by modeling the effects of nucleosynthetic anomalies.

Table S3: Decomposing mass-dependent and mass-independent effects for the IVB iron meteorite Cape of Good Hope using 'absolute' Mo isotope compositions (for details see text and Fig. S3)

nucleosynthetic anomalies (internally normalized to $^{97}Mo/^{95}Mo$; red line in Fig. S3a)	$\varepsilon^{92}Mo$	0.14	calculated isotope abundances	^{92}Mo	14.7342
	$\varepsilon^{94}Mo$	0.05		^{94}Mo	9.2130
	$\varepsilon^{95}Mo$	0		^{95}Mo	15.8923
	$\varepsilon^{96}Mo$	-0.74		^{96}Mo	16.6705
	$\varepsilon^{97}Mo$	0		^{97}Mo	9.5685
	$\varepsilon^{98}Mo$	-0.23		^{98}Mo	24.2252
	$\varepsilon^{100}Mo$	1.06		^{100}Mo	9.6963
			mass-independent effect on $\delta^{98/95}Mo$	$\delta^{98/95}Mo$	-0.023
isotope abundances with SRM composition in deconvolution	^{92}Mo	14.7400	abundances with IVB abundances in deconvolution (normalizing to SRM gives blue line in Fig. S3a)	^{92}Mo	14.7393
	^{94}Mo	9.2147		^{94}Mo	9.2145
	^{95}Mo	15.8939		^{95}Mo	15.8937
	^{96}Mo	16.6717		^{96}Mo	16.6706
	^{97}Mo	9.5675		^{97}Mo	9.5677
	^{98}Mo	24.2208		^{98}Mo	24.2212
	^{100}Mo	9.6914		^{100}Mo	9.6931
apparent fractionation (green line in Fig. S3b)	$\delta^{98/95}Mo$	-0.25	mass-dependent+mass-independent fractionation (from blue line in Fig. S3a)	$\delta^{98/95}Mo$	-0.22
			mass-dependent fractionation (black line in Fig. S3b)	$\delta^{98/95}Mo$	-0.20
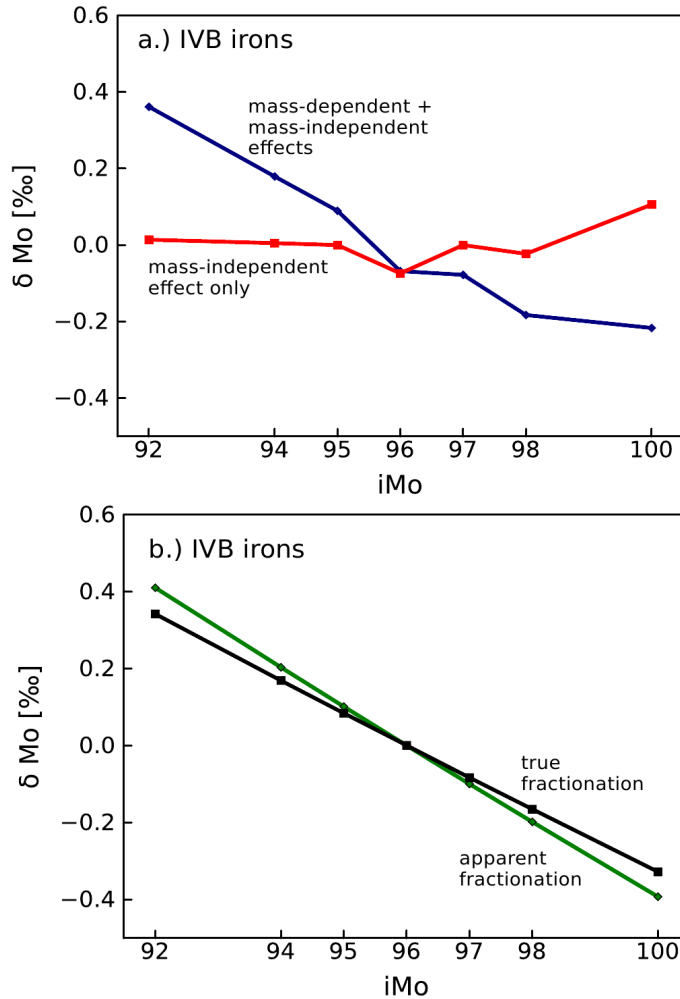
Figure S3. Effect of nucleosynthetic anomalies on stable Mo isotope fractionation exemplified for the IVB iron meteorite Cape of Good Hope. a.) Blue line represents the δ^iMo values relative to the SRM 3134 standard as obtained from using the internally normalized values in the inversion, including mass-dependent and mass-independent Mo isotope variations. Red curve is the pure mass-independent part as obtained from the unspiked run for normalization to ^{97}Mo/^{95}Mo (Burkhardt et al., 2011). b.) The true mass-dependent fractionation is the difference between the blue and the red curve, represented by the black line. Also shown are the δ^iMo values calculated in the double spike inversion referenced to the composition of the SRM 3134 standard (green line). For Cape of Good Hope the difference between these two results corresponds to ~0.05‰ $\delta^{98/95}$Mo, indicating that for this sample the measured $\delta^{98/95}$Mo of -0.25 needs to be corrected upwards to $\delta^{98/95}$Mo$_{corrected}$ = -0.20.

S2.3 Investigating the effect of decomposing mass-dependent and mass-independent effects on absolute Mo isotope compositions

In order to further test the accuracy of our results we designed a calculation (performed in Matlab) to investigate under what conditions mass-dependent and mass-independent contributions to isotope abundances can be accurately decomposed. The aim of this calculation is to prove that our data reduction scheme yields accurate decomposition of mass-dependent and mass-independent components. In addition, we

have explored under what conditions the method would break down. The code does the following: starting with the SRM abundances as a 'reference' material it adds mass-independent anomalies using certain multiplication factors. Further, it adds a certain mass-dependent fractionation to the reference material, based on a fractionation factor (α). Then the code combines the mass-independent and mass-dependent contributions to generate abundances of a 'sample', and it does this twice: once first adding a mass-independent contribution to the reference followed by a mass-dependent fractionation event (so mass-dependent fractionation of a 'sample' that already had a mass-independent signature), and once the other way around. After this, our double spike is added to these 'sample' abundances with a molar spike proportion of 0.47, followed by some realistic instrumental fractionation assuming an exponential law. Then it does a double spike deconvolution using the two methods used for our real samples: (1) the first one uses the SRM abundances as a reference in the deconvolution, and (2) the second one uses the abundances of the 'sample' with its mass-independent contribution (*i.e.*, the isotope composition that would be obtained from an internally normalized, unspiked run) as a reference.

The code always modeled a two stage 'process', one mass-dependent and one mass-independent process. The variables include: (1) magnitudes of mass-independent contribution; (2) magnitude of mass-dependent fractionation; (3) adding a mass-independent contribution in the form of epsilon values derived from internal normalization to ^{98}Mo/^{96}Mo, ^{92}Mo/^{98}Mo and ^{97}Mo/^{95}Mo; (4) the order of the events. Of course, in all cases, the inversion with SRM abundances as reference fails to reproduce the input value of the mass-dependent fractionation factor α, due to the mass-independent effects. For the inversion with the 'sample' abundances as a reference, the conditions that lead to accurate decomposition of mass-dependent and mass-independent contributions are as follows: *with realistic values for mass-independent (epsilon range) and mass-dependent contributions (sub-permil to permil range), (i) any effects of different normalizations are so small that they would be undetectable; and (ii) the order of adding effects (i.e., first mass-independent or first mass-dependent) also does not lead to detectable differences.* However, for extreme values of mass-independent contributions (percent range anomalies, as opposed to epsilon range) the order of processes matters: If there is first a mass-independent contribution and then a mass-dependent process, the decomposition is accurate in all scenarios. The other way around, however, the extreme cases fail. For instance, for a mass-dependent fractionation event equivalent to $\delta^{98/95}$Mo = -6.22‰ (i.e. α = 0.20) followed by a mass-independent event that produced the equivalent of an *s*-process deficit of 0.5% (for instance, for internal normalization to $^{97/95}$Mo this would correspond an anomaly in ϵ^{92}Mo of 100; *cf.* Fig. S2), the decomposition gives $\delta^{98/95}$Mo= -6.31‰ (or α= 0.1987), which is 0.09‰ too small.

Given the small range of nucleosynthetic anomalies observed in bulk planetary samples (epsilon range), these modeling results provide an additional proof of the accuracy of our correction schemes and the resulting Mo isotope data.

References

Arlandini, C., Käppeler, F., Wisshak, K. (1999): Neutron capture in low-mass asymptotic giant branch stars: cross sections and abundance signatures. *Astrophysical Journal, 525*, 886-900.

Burkhardt, C., Kleine, T., Oberli, F., Pack, A., Bourdon, B., Wieler, R. (2011): Molybdenum isotope anomalies in meteorites: Constraints on solar nebula evolution and origin of the Earth. *Earth and Planetary Science Letters, 312*, 390-400.

Dauphas, N., Marty, B., Reisberg, L. (2002): Molybdenum evidence for inherited planetary scale isotope heterogeneity of the protosolar nebula. *Astrophysical Journal, 565*, 640-644.

Lu, Q., Masuda, A. (1994): The isotopic composition and atomic weight of molybdenum. *International Journal of Mass Spectrometry and Ion Processes, 130*, 65-72.

Niederer, F.R., Papanastassiou, D.A., Wasserburg, G.J. (1985): Absolute isotopic abundances of Ti in meteorites. *Geochimica et Cosmochimica Acta, 49*, 835-851.

Rudge, J. F., Reynolds, B. C., Bourdon, B. (2009): The double spike toolbox. *Chemical Geology*, *265*, 420-431.